buildings

MDPI

Article

Analysis of a Stress-Strain State of a Cylindrical Tank Wall Vertical Field Joint Zone

Nurlan Zhangabay [1], Ulanbator Suleimenov [2], Akmaral Utelbayeva [3,*], Alexandr Kolesnikov [4,*], Kanat Baibolov [5], Kuanysh Imanaliyev [2], Arman Moldagaliyev [6], Galymzhan Karshyga [7], Bolat Duissenbekov [2], Roman Fediuk [8,9,*] and Mugahed Amran [10,11]

[1] Department of Construction and Construction Materials, M. Auezov South Kazakhstan University, Avenue Tauke Khan, 5, Shymkent 160012, Kazakhstan
[2] Department of Architecture, M. Auezov South Kazakhstan University, Avenue Tauke Khan, 5, Shymkent 160012, Kazakhstan
[3] Department of Chemistry, M. Auezov South Kazakhstan University, Avenue Tauke Khan, 5, Shymkent 160012, Kazakhstan
[4] Department of Life Safety and Environmental Protection, M. Auezov South Kazakhstan University, Avenue Tauke Khan, 5, Shymkent 160012, Kazakhstan
[5] Department of Engineering, Peoples Friendship University Named after Academician A. Kuatbekov, Street, Tolebi n/n, Shymkent 160012, Kazakhstan
[6] Department of Mechanics and Mechanical Engineering, M. Auezov South Kazakhstan University, Avenue Tauke Khan, 5, Shymkent 160012, Kazakhstan
[7] Department of Architecture and Construction Production, Qorqyt Ata Kyzylorda University, Street Aiteke Bi 29A, Kyzylorda 160014, Kazakhstan
[8] Polytechnic Institute, Far Eastern Federal University, 690922 Vladivostok, Russia
[9] Peter the Great St. Petersburg Polytechnic University, 195251 Saint Petersburg, Russia
[10] Department of Civil Engineering, College of Engineering, Prince Sattam Bin Abdulaziz University, Alkharj 16273, Saudi Arabia
[11] Department of Civil Engineering, Faculty of Engineering and IT, Amran University, Amran 9677, Yemen
* Correspondence: mako_01-777@mail.ru (A.U.); kas164@yandex.kz (A.K.); fedyuk.rs@dvfu.ru (R.F.)

Abstract: In the study, experimental and theoretical studies were carried out to assess the influence of the vertical mounting joint zone of the tank on the stress-strain state of the defect zone. Thus, experimental tests of models of a tank wall fragment with an imperfection of the mounting joint evaluated the stress-strain state of the mounting joint zone and established the dependence of the stress concentration in the joint zone on the deflection, the width of the zone and the thickness of the tank wall. It is shown that with a 50 mm bending boom, the annular stresses increase by 1.3 times than with a 30 mm bending boom and the meridional stresses increase by 1.16 times. The same nature of the increase is observed with the stress concentration indicator. By numerical analysis of the stress-strain state of tanks with joint imperfections in the ANSYS medium, the stress-strain state of the tank is estimated for various values of the joint bending parameters ς and ξ. The dependences of the stress concentration coefficient on the geometric dimensions of the imperfection, radius and thickness of the tank wall are also obtained. From the results of calculating the stress concentration coefficient, with an increase in the dimensionless parameters ς and ξ, the values of the stress concentration coefficient K_σ increase by 1.35 times. As a result of the calculations, an interpolation polynomial (5), approximating the stress concentration coefficient K_σ, is obtained, which can be used to estimate the strength, durability and residual resource of the tank. In addition, the obtained results can be used to normalize the limiting dimensions of the imperfection of the joint and to establish the values of the coefficient, taking into account the peculiarities of the work of structures at stress concentrations.

Keywords: tank; stress concentration; joint zone; wall vertical field; experimental study; numerical method; modeling

check for updates

Citation: Zhangabay, N.; Suleimenov, U.; Utelbayeva, A.; Kolesnikov, A.; Baibolov, K.; Imanaliyev, K.; Moldagaliyev, A.; Karshyga, G.; Duissenbekov, B.; Fediuk, R.; et al. Analysis of a Stress-Strain State of a Cylindrical Tank Wall Vertical Field Joint Zone. *Buildings* **2022**, *12*, 1445. https://doi.org/10.3390/buildings12091445

Academic Editor: Humberto Varum

Received: 17 August 2022
Accepted: 6 September 2022
Published: 14 September 2022

1. Introduction

In the new century, more and more serious attention is being paid to the country's security issues at all levels of legislative and executive power. A special key place is occupied by the problem of increasing the efficiency and safety of oil and oil products' storage, which have very specific properties. The main element of oil and oil products' storage points and bases is large-sized steel vertical cylindrical tanks, which involves construction and maintenance intensification. At the same time, vertical cylindrical tanks are classified as especially critical structures, the destruction of which can lead to environmental disasters, significant material costs, and human casualties. Therefore, tanks' construction and operation should be based on sound scientific, technically feasible, fundamentally new designs and economically viable solutions. In addition, in order to limit energy consumption, specialists are currently conducting various studies in the field of energy saving and development of alternative energy sources [1,2].

It is known that the most common causes of accidents and emergency situations in all types of tanks (steel, concrete, reinforced concrete, vertical, horizontal, etc.) are stress concentrators, in combination with adverse operational impacts and various tank design options have been considered, including steel, concrete, horizontal and vertical. Tank designs take into account the material's characteristics, as well as ways to improve the strength properties of the materials themselves [3–20]. In this regard, this paper considers the issue of a comprehensive study of a cylindrical tank wall vertical field joint zone's true stress-strain state, an improved method for calculating limit states, and establishing the factor values, taking into account the features of work at stress concentrations. The relevance of the problem under consideration is also due to a sharp decrease in the volume of new construction, which led to a noticeable "aging" of the tank farm and an increase in the proportion of tanks whose technical condition is close to the limit and requires specific measures to ensure the trouble-free operation of cylindrical steel tanks.

The authors Wang et al. [21] present the results of modeling the operation of steel cylindrical tanks filled with liquid. Fan Y. et al. [22] present a numerical analysis method. Martynenko G. et al. [23] note that a typical tank design has a wall that is modeled by a thin shell. Wang, Zh. et al. [24] study the buckling of a tank wall at a constant external pressure. It is shown that the presence of initial defects in the design significantly reduces the strength of the tanks. Rastgar et al. [25] consider the issues of repairing dents with carbon fiber reinforcement in order to restore the lost bearing capacity. Fatma M. et al. [26] provide the results of a strength assessment of a cylindrical shell wall with a dent, taking into account the stress concentration in the defect zone, where the issue of stress concentrations in the defect was also not considered, and the shape and geometric dimensions of defects in the form of dents were not taken into account [27].

Bannikov R. et al. [28] only consider the problem of assessing the technical condition of steel tanks with a defect in the form of a dent, without taking into account the weld. Dmitrieva et al. [29] mainly consider the issue of durability of the structure from the corrosion process of a vertical steel tank shell. Mariusz et al. [30] highlight the problem of the increase in the corrosion rate over time, and also analyze the residual life calculation. In the work of Song, Z. et al. [31], the oscillatory sliding contact between a rigid rough surface and an elastic-plastic half-space was considered in the context of numerical modeling. Hagihara S. et al. [32] present a method for calculating the J-integral and T*integral in a framework of the EFG method. The proposed method is applied to both a stationary crack problem and a stable crack growth problem. In the work of Sun Jichao [33], through static analysis, the resultant force of particles in rock fissures is extruded by rock on both sides. Zhang Y et al. [34] attempted to simulate girth welded pipelines with various corroded depths and lengths in order to compare it with offshore pipeline design manuals. Based on the numerical results, the influence of corrosion defect parameters on remaining strengths were investigated for girth welded pipelines. Yi Dake et al. [35] provide a method for assessing the ability to destroy a practical pipeline subject to large plastic deformation.

As the results of the above analysis of vertical cylindrical tanks' operation showed, the problems of angular strains in scroll tank field joints require significant improvement, since the angular strains in the tank wall field joint significantly affect the stress-strain state in the joint zone, lead to a significant stress concentration in the joint zone, and under conditions of re-variable loads, reduce the tank performance as a whole. Considering the foregoing information, the research purpose involves the experimental and theoretical assessment of a cylindrical tank wall vertical field joint zone and the stress concentration dependence identification on the joint imperfection geometric dimensions, which, in the future, will allow us to predict vertical steel tanks' service life. The research results can be used in steel vertical cylindrical tanks' design and construction.

2. Materials and Methods

At the first stage, taking into account the features of modeling thin-sheet cylindrical shells, the technical feasibility of manufacturing a model, and also taking into account the possibility of applying a load and measuring the experimental parameters, a modeling scale of 1:10 was adopted to the full-scale structures of a vertical cylindrical tank with a volume of 2000 m^3, according to a standard design [36,37]. Modeling was carried out on the basis of the theory of similarity and dimensions.

To carry out the experiments, a large-scale model of a vertical cylindrical tank's vertical scale joint zone, with a geometric imperfection in the form of angularity, was made.

The overall model dimensions were 1200 × 850 × 550 mm. The field joint was formed from two 2 mm thick VSt3sp grade steel sheets, rolled along a radius of 1520 mm and welded at the joint. The joint imperfection in the form of depression was modeled by rolling the sheet edge along a radius of 30 mm and 50 mm and the angularity formation in the form of a "heart". The geometric scheme of the wall imperfection in the field joint zone in the model is presented in accordance with Figure 1.

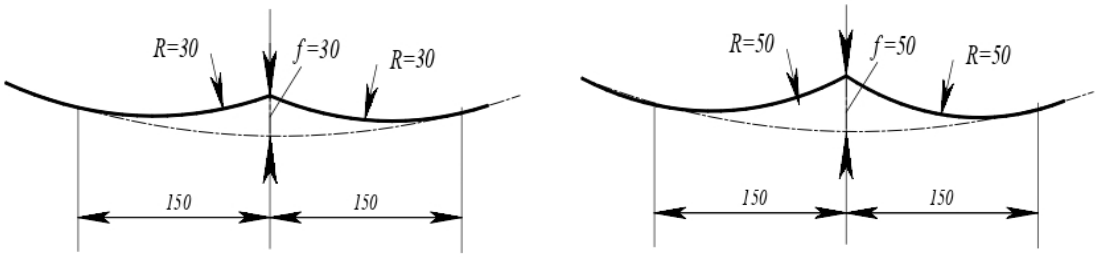

Figure 1. Geometric dimensions of the joint imperfection in the model.

The model's back side was made of a thick-walled pipe 4 mm thick. The model's bottom and roof were made of metal plates 4 mm thick.

The chemical composition of steel was determined by the gas volume method according to [38]. The mechanical characteristics of steel were determined by standard tests of samples according to [39] and are given in accordance with Table 1.

Table 1. Mechanical characteristics of the model's body material.

Steel	Mechanical Properties		Mn	Si	S	P	Cr	Ni	Cu
	Yield Strength, MPa	Breaking Strength, MPa							
VStp	240–245	370–480	≤0.65	0.15–0.30	0.050	0.040	≤0.30	≤0.30	0.30

To simulate overpressure, a fitting with a diameter of 15 mm was placed on the model roof for air supply by a compressor and a branch pipe for installing a spring pressure gauge. The tightness of the models was tested with compressed air at a pressure of 0.02 kg/cm^2.

To place dial indicators on the model, a rigid profile was additionally fixed, on which dial indicators were mounted with special clamps.

The methodology for conducting experiments on reduced models defined the procedure and principles for conducting the tests that solve the issues of creating effects that are adequate to real loads, choosing and using equipment, apparatus and instruments corresponding to the tests, recording and processing the results obtained, and assessing measurement errors. The research method, measuring instruments, devices and equipment were chosen in accordance with the tasks faced by the experimental research.

Relative strains of the model wall were measured by strain-measuring instruments [40–49]. As sensing devices for measuring relative strains, single-element, loop strain gauges with a 10 mm foil base were used. The strain gauges were mounted with Tsiacrin-30 glue, which is factory-made and does not require heat treatment.

The TsTM-5 strain-measuring set and AID-4M automatic strain gauge with automatic balancing of bridges (half-bridges), completed with an AP-1 automatic switch, served as the recording equipment.

To register the vertical field joint axis movements in the characteristic four sections, ICH-04 dial indicators with a division value of 0.01 mm were installed, which were fixed on special brackets, in accordance with Figure 2. The strain gauges were glued along four characteristic sections (C-I, C-II, C-III, C-IV) along the model height, in accordance with Figure 3. For each section, 6 measurement points were considered. The strain gauges were glued in such a way that at one point, it was possible to measure the hoop and axial stresses in the model wall. In total, measurements were taken from 32 active and 16 control strain gauges in the experiments. In this case, the total test zone height was taken equal to 600 mm, and its width was 300 mm.

Figure 2. Placement of ICH-04 dial indicators.

The model is symmetrical with respect to the joint axis; in connection with this, strain gauges were glued only on half of the model, and only control strain gauges were glued to the second half.

The shell was loaded stepwise from 0 to 0.04 kg/cm^2 and then the model was unloaded stepwise. At each step, the relative strains were measured in four sections, as well as the

weld point displacements, both under loading and unloading of the model. The obtained data were processed in compliance with the procedures and methods for solving practical problems of statistics, when the measured values are random and distributed according to the normal law in accordance with the standard [50–60].

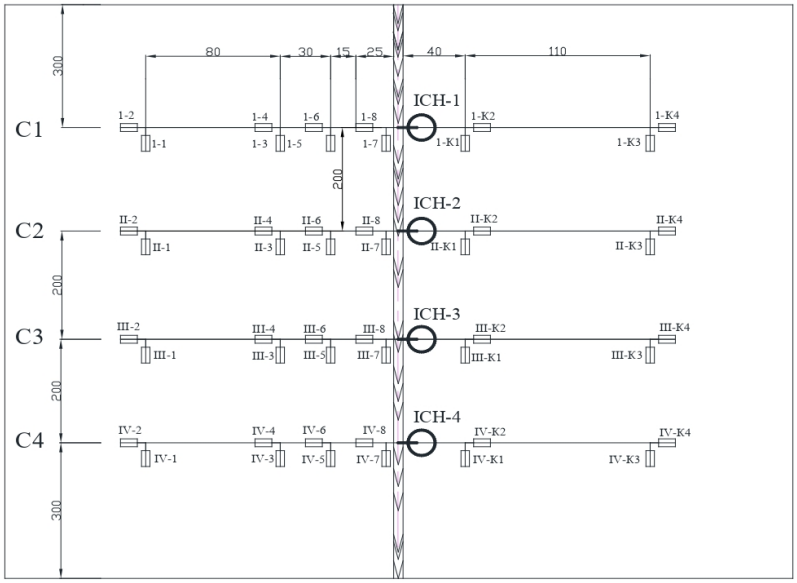

Figure 3. Placement of strain gauges and dial indicators in the field joint zone.

The pressure in the model was created by a compressor and controlled by a spring pressure gauge MVTP-160, with a division value of 0.02 MPa. The block diagram for testing the models, instrumentation and data determined in the experiment are presented in accordance with Figure 4. According to the relative strains measured during the experiment, the stresses were recalculated and the stress-strain state of the wall in the field joint zone was analyzed.

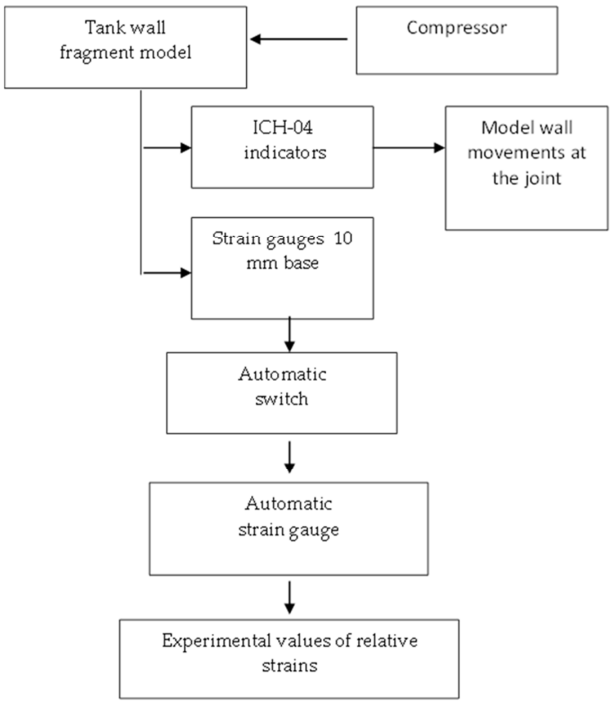

Figure 4. Block diagram of the experiment.

The stress concentration factors were determined by the ratio of the maximum local stresses in the joint imperfection zone to the nominal stresses in the defect-free tank body zone. The dependence of the stress concentration factor on the geometric dimensions of the imperfection, as well as data on the stress-strain state of the wall, were used in further theoretical studies. The developed method of the experimental study of the tank field joint's imperfection effect on the wall stress-strain state on the reduced models allowed us to fully solve the tasks set for the research. The data obtained on the true stress-strain state of the field joint zone with geometric shape imperfections allowed us to evaluate the geometric imperfection dimension effect on the stress concentration.

At the second stage, the typical vertical cylindrical tank design with a volume of 3000 m^3 was considered, filled with liquid with an imperfection zone in the field welded joint along the entire tank height, in accordance with Figure 5 [61].

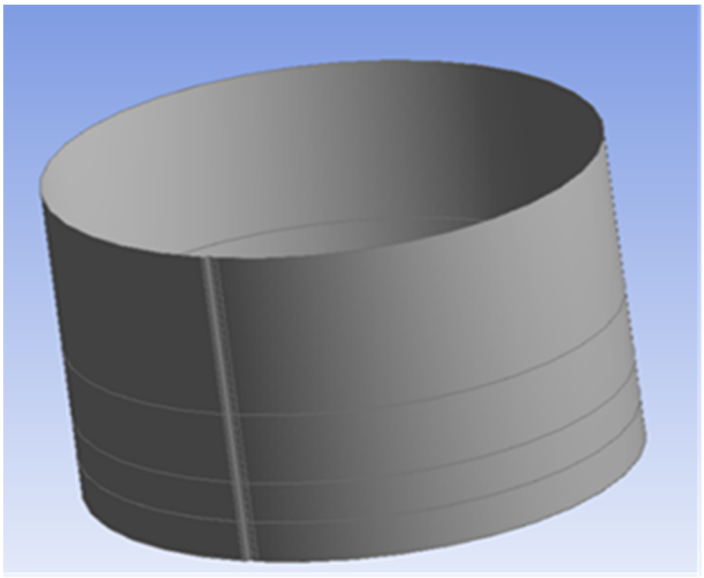

Figure 5. General view of the tank, taking into account the field joint [61].

For numerical simulation of the tank's stress-strain state caused by the internal pressure action, the ANSYS software package was used. The stress-strain state perturbations in the joint zone are described by the stress concentration factor K_σ.

Experience in the tank operation has shown that the stress-strain state of the tank wall in the field joint zone depends on the geometric imperfections of the joint itself. Such imperfections include the angularity under the action of a uniformly distributed pressure, determined by the joint deflection f, the angularity width a, the radius R and the tank wall thickness t.

Based on the hypothesis described in the works, the stress concentration factor depends on two dimensionless parameters f/t and $a/\sqrt{RT}$ where t—the shell thickness; f—the joint bend depth; R, t—the tank radius and thickness.

The final expression for the stress concentration coefficient is obtained (K_σ^T) in the following form:

$$K_\sigma^T \approx \alpha\left(\frac{f}{t}; a/\sqrt{RT}\right) \quad (1)$$

As a result of the calculations of the tank stress-strain state for various values of the dent parameters f/t and $a/\sqrt{RT}$, polynomials that approximate the stress concentration factor K_σ were constructed.

These approximating polynomials for the factor K_σ are extremely effective for carrying out estimated calculations of the tank body stress-strain state with arbitrary geometry and with arbitrary geometric dimensions of the field joint imperfections.

The design of a typical vertical cylindrical tank with a volume of 3000 m^3 and the stress-strain state of the tank wall of variable thickness were considered in accordance with the paper [61]. The tank material elasticity modulus and Poisson's ratio were taken as follows: $E = 2.1 \times 10^{11}$ Pa; $v = 0.3$. One must assume that the tank was completely filled ($h = 11.92$ m) with the density of the liquid $\gamma = 1000$ kg/m^3. The adequacy of the results was assessed by comparing the stress concentration factor values obtained by calculations in the ANSYS and the values obtained from the polynomials, which take into account the cylindrical tank wall field joint imperfections.

3. A Cylindrical Tank Wall Vertical Field Joint Zone's Stress-Strain State Research Results

3.1. Experimental Research

In accordance with the developed methodology for conducting experiments, at the initial stage, the annular and meridional deformation components were measured in the characteristic sections of the tank field joint fragment model. An analysis of the hoop stress diagrams in the model wall in the field joint zone at various values of the camber, in accordance with Figure 6, showed that at the level of 500 mm from the model bottom, at the level of the main nominal stresses of 60.8 MPa, the maximum stresses in the joint zone amounted to 276 MPa, with a camber of 30 mm and 358 MPa with a camber of 50 mm.

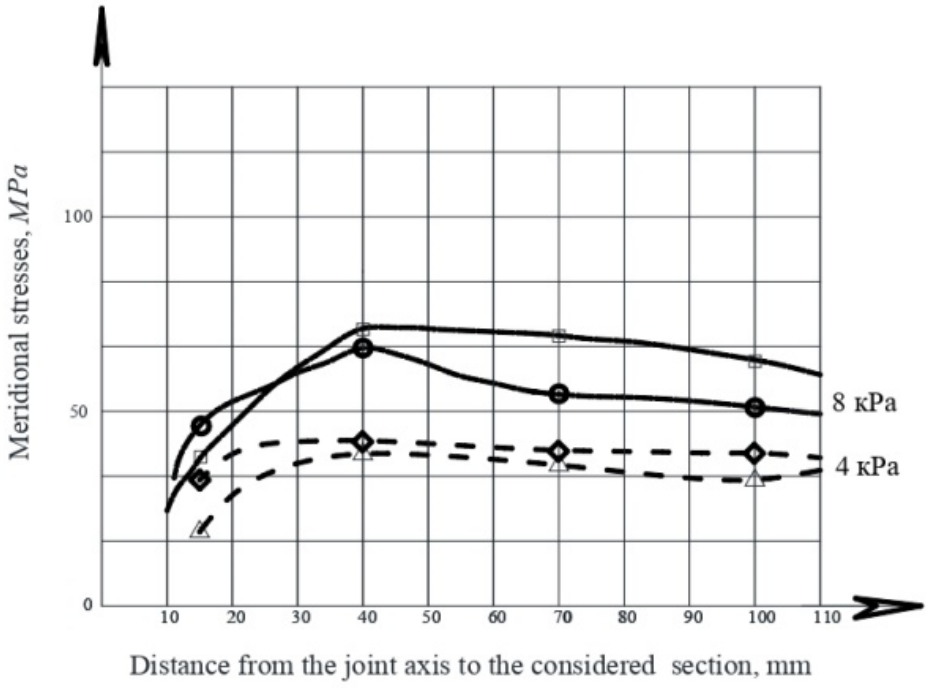

_____ load is 8kPa; _ _ _ _ _ _ load is 4kPa

Figure 6. Distribution of the meridional stresses in the joint zone with the wall bend in the joint equal to 30 mm and 50 mm.

The facts established by the tests prove the assumption of significant concentrations in the field joint zone with a defect in the form of angularities, and also indicates the decisive influence on the stress concentration in the joint zone of such imperfection parameters as the camber and the reduced width of the bend zone. At significant values of the camber at the boundary sections of the bend, the hoop stresses are somewhat lower than the nominal ones, which, apparently, are associated with the expanding action of the bent wall part. The hoop stress diagram curves (Figure 7) indicate the characteristic stress concentration, which was observed at points located closer to the wall bend line.

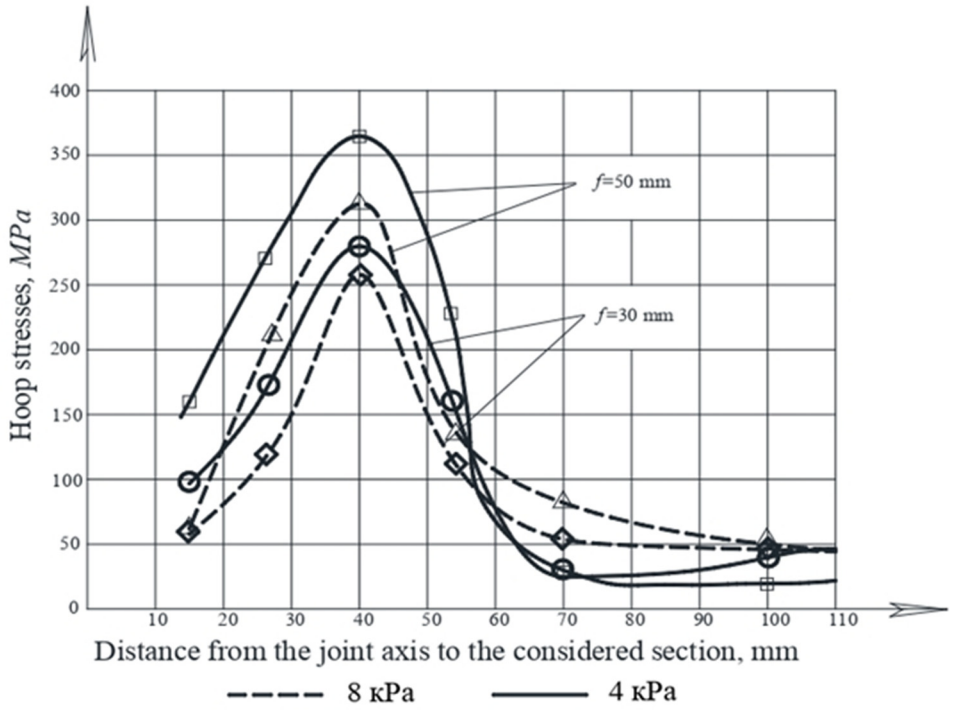

Figure 7. Distribution of the hoop stresses in the joint zone with the wall bend in the joint point *f* equal to 30 mm and 50 mm.

The meridional stress diagrams, constructed on the basis of experimental data, in accordance with Figure 8, show that the bend of the field joint does not significantly affect the meridional stress distribution in the joint zone.

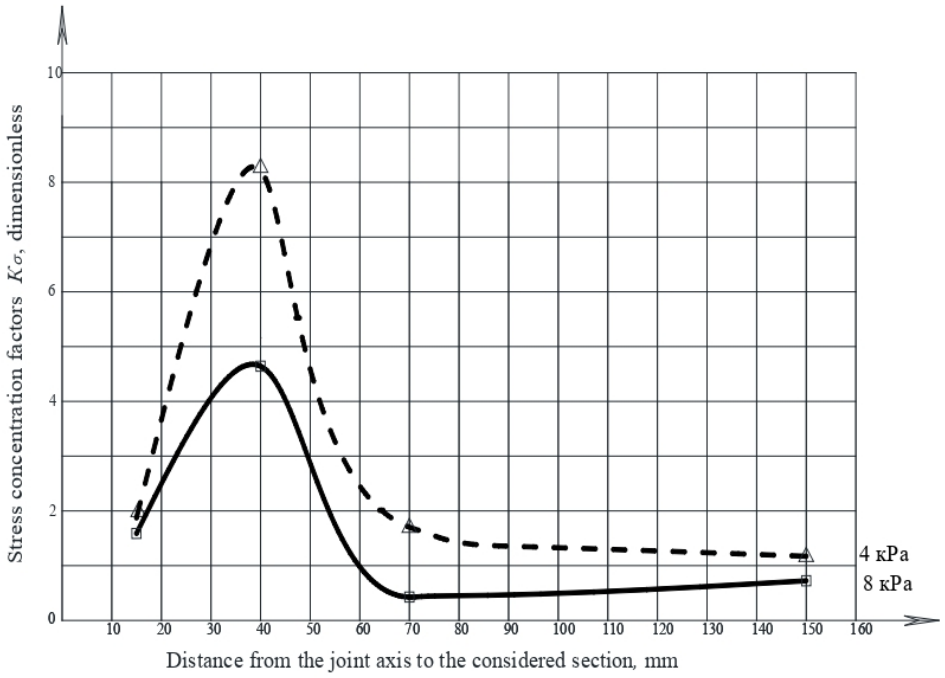

Figure 8. The hoop stress concentration in the field joint zone of the wall, with a bend of 30 mm in section C-3.

There is evidence of some (1.1 and 2.3 times) increase in the stresses in the bend place and its uniform redistribution. An increase in the bend *f* from 30 mm to 50 mm does

not have a significant effect on the stress distribution in the joint zone. The maximum meridional stress value at an internal pressure of 8 kPa and a bend of 30 mm was 67 MPa, and at a bend of 50 mm, it was 78 MPa. The nominal meridional stress level was 32 MPa.

According to the experimental data, the hoop and meridional stress concentrations in the joint zone were estimated, in accordance with Figures 8–11, depending on the bend value and internal pressure in the model.

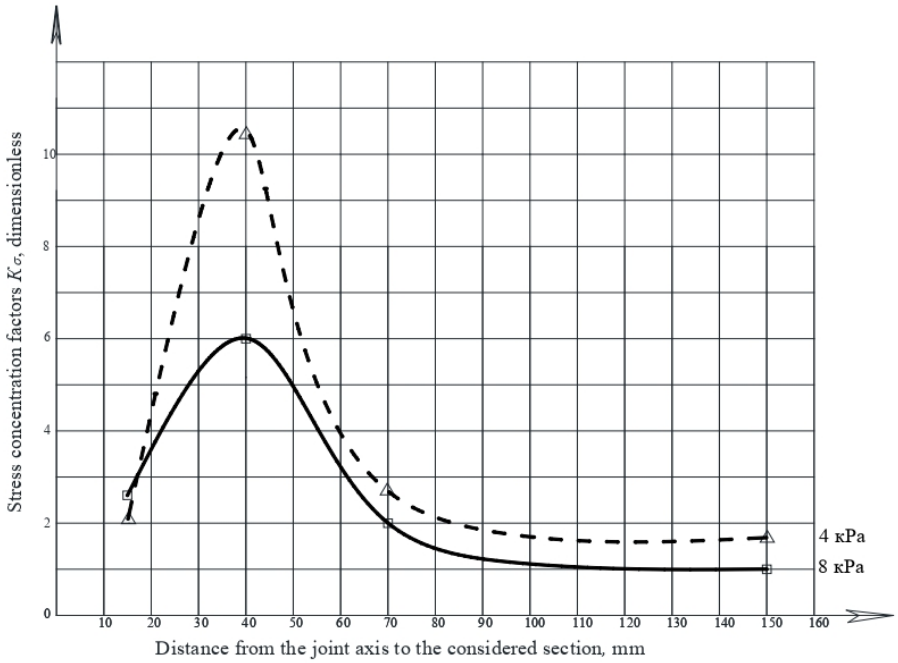

Figure 9. The hoop stress concentration in the field joint zone of the wall with a bend of 50 mm in section C-3.

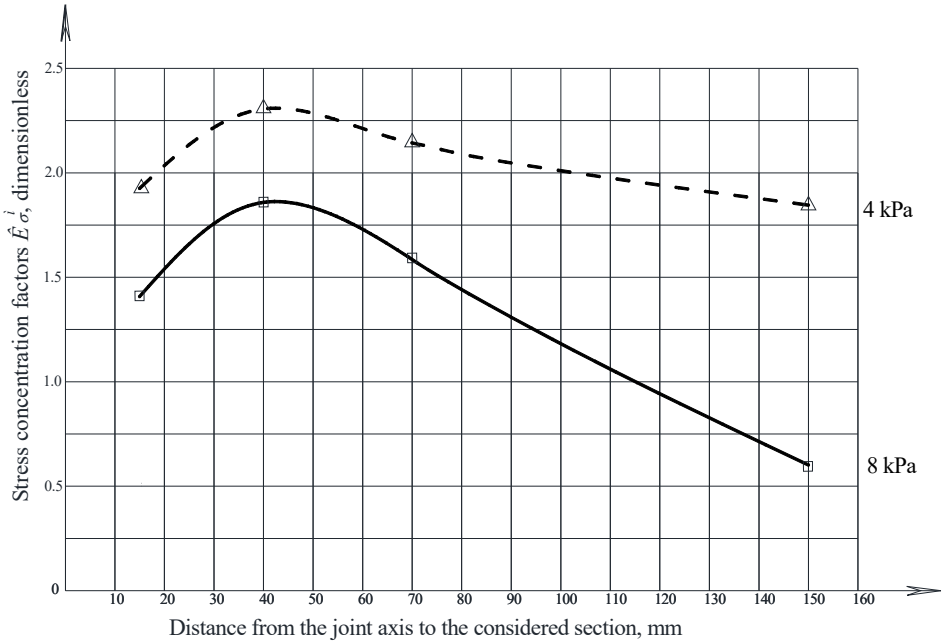

Figure 10. The meridional stress concentration in the field joint zone of the wall with a bend of 30 mm in section C-3.

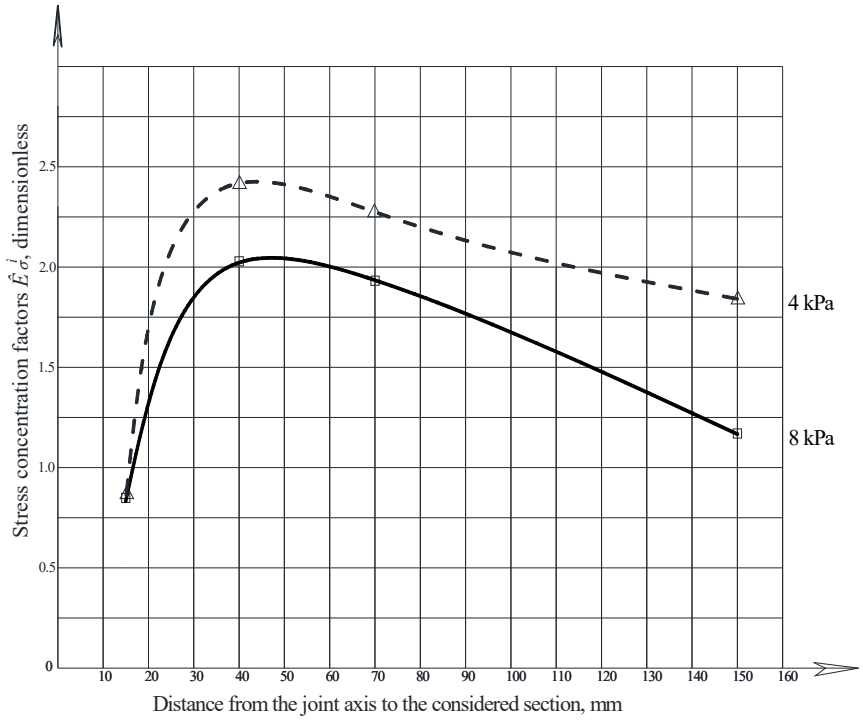

Figure 11. The meridional stress concentration in the field joint zone of the wall with a bend of 50 mm in section C-3.

The maximum stress concentration in the joint zone was 4.54 for the model with a bend of 30 mm, and 5.89 for a camber of 50 mm.

An analysis of the graphs, Figures 8–11, shows that with an increase in internal pressure due to the field joint zone's bend straightening, a decrease in the hoop stress concentration value is observed.

A qualitatively similar distribution of the hoop and meridional stresses in the wall field joint zone was also observed when a tank with a volume of 3000 m^3 was tested.

Figures 12 and 13 show the hoop and meridional stress diagrams in the field joint zone of a full-scale tank wall with a bend of 20 mm, 29 mm and 36 mm.

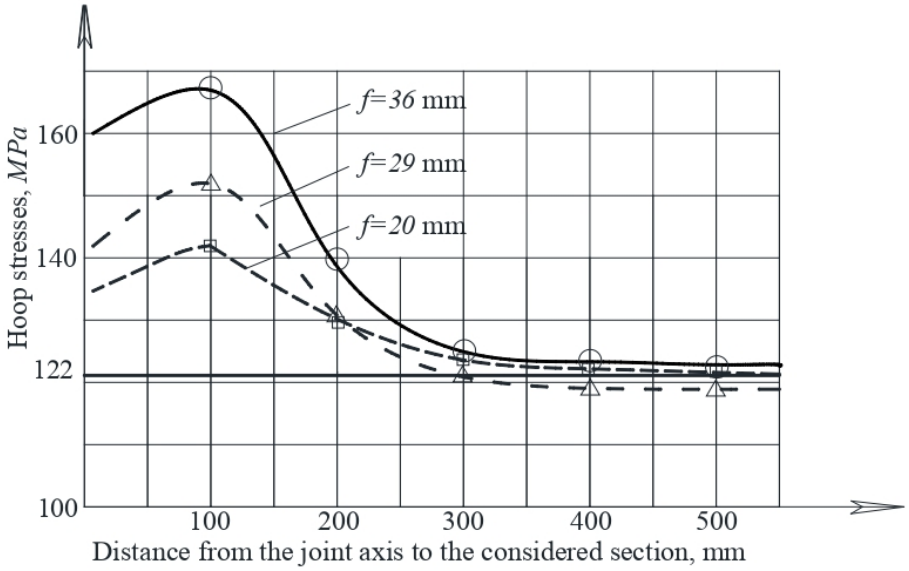

Figure 12. The hoop stress diagrams in the tank wall field joint zone with a volume of 3000 m^3 with bend: □ f = 20 mm; △ f = 29 mm; ○ f = 36 mm.

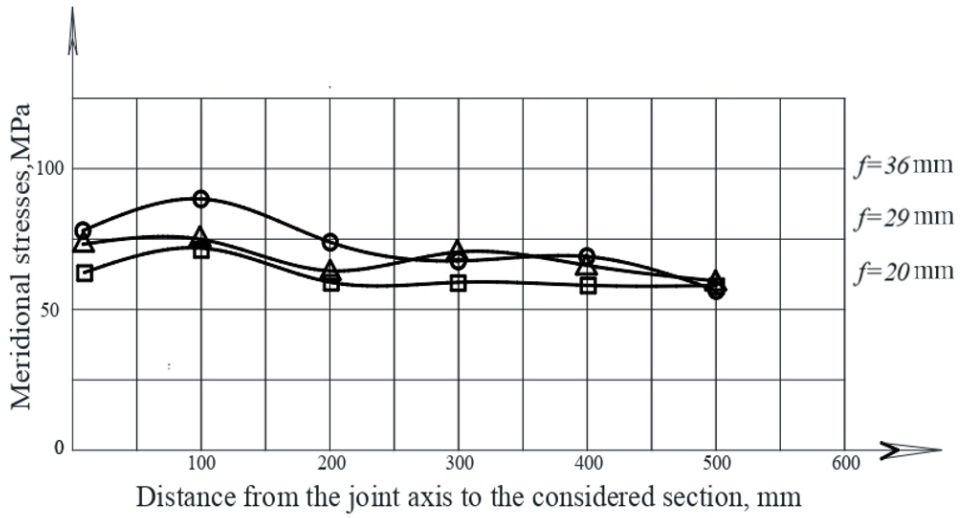

Figure 13. The meridional stress diagrams in the tank wall field joint zone with a volume of 3000 m^3 with bend: □ f = 20 mm; △ f = 29 mm; ○ f = 36 mm.

Tests of the operated tank showed that the maximum hoop stresses at the level of nominal stresses of 122 MPa and the field joint bend of 36 mm were 168 MPa, at 29 mm, they were 153 MPa; at 20 mm, they were 141 MPa, which do not exceed the normative yield strength values of the 09G2S grade steel tank wall, equal to 295 MPa.

The maximum meridional stresses were as follows: at the bend of 36 mm—83 MPa, 29 mm—75 MPa and 20 mm—72 MPa.

The tests established that the initial imperfection shape and its geometric dimensions significantly affect the wall stress-strain state in the field joint zone.

Based on the experimental stress value results, the stress concentration factors were estimated for various field joint bend values. The calculation results are shown in accordance with the graphs of Figure 14.

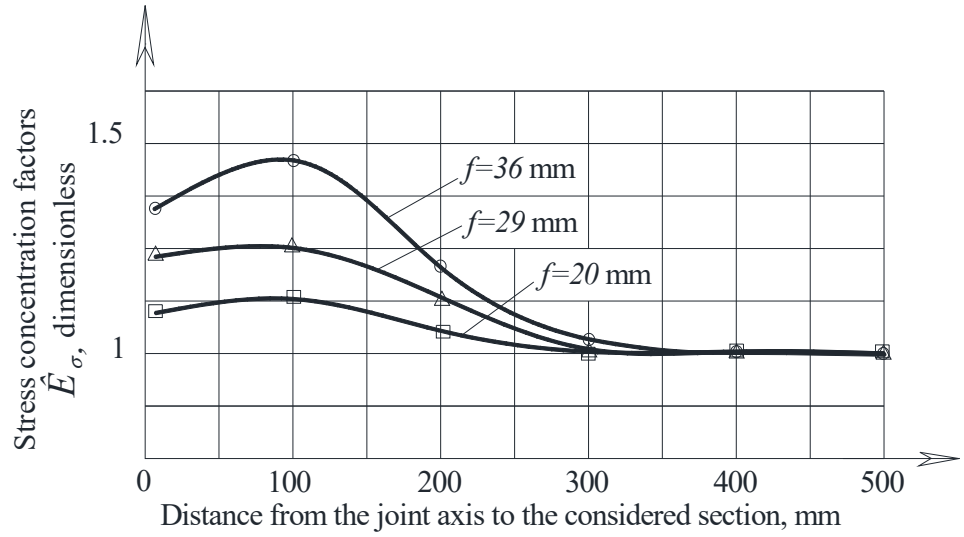

Figure 14. Stress concentration in the operated full-scale tank wall field joint zone with bend: □ f = 20 mm; △ f = 29 mm; ○ f = 36 mm.

The stress concentration in the tank wall joint zone with bends of 36 mm, 29 mm and 20 mm was 1.38, 1.25 and 1.16, respectively.

The conducted studies allowed us to once again be convinced of the importance of taking into account the tank wall joint zone imperfection, as well as assessing the stress concentration in the wall imperfection zone.

3.2. Theoretical Research

At the second stage, numerical analysis of the stress-strain state of tanks with joint imperfections was carried out in the ANSYS environment.

The tank body was divided into shell finite elements with a variable mesh. In the region of the dent, the mesh sizes decreased. The lower tank belt finite elements mesh is presented in accordance with [61]. The stress-strain state calculation convergence with a decrease in the finite element mesh size was investigated. For this, the tank stress-strain state was calculated for various finite element mesh sizes, and the required finite element mesh was selected based on the comparison results. The results of the calculations of equivalent stresses on the outer tank surface for various values of the tank wall field joint imperfection bend and width are shown in accordance with Figures 15–18.

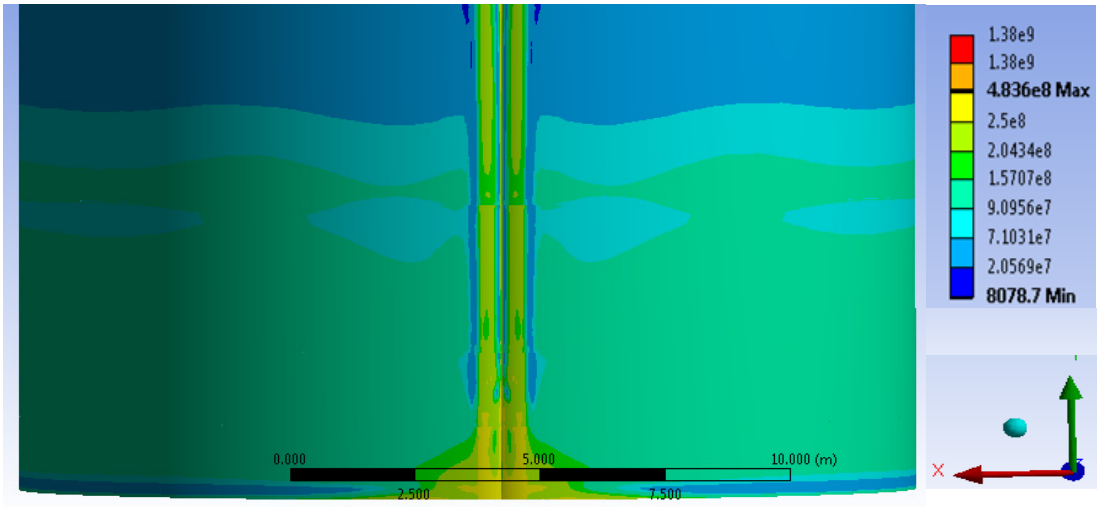

Figure 15. Distribution of equivalent stresses in the field joint zone with the joint imperfection at a = 50 cm; f = 1 cm.

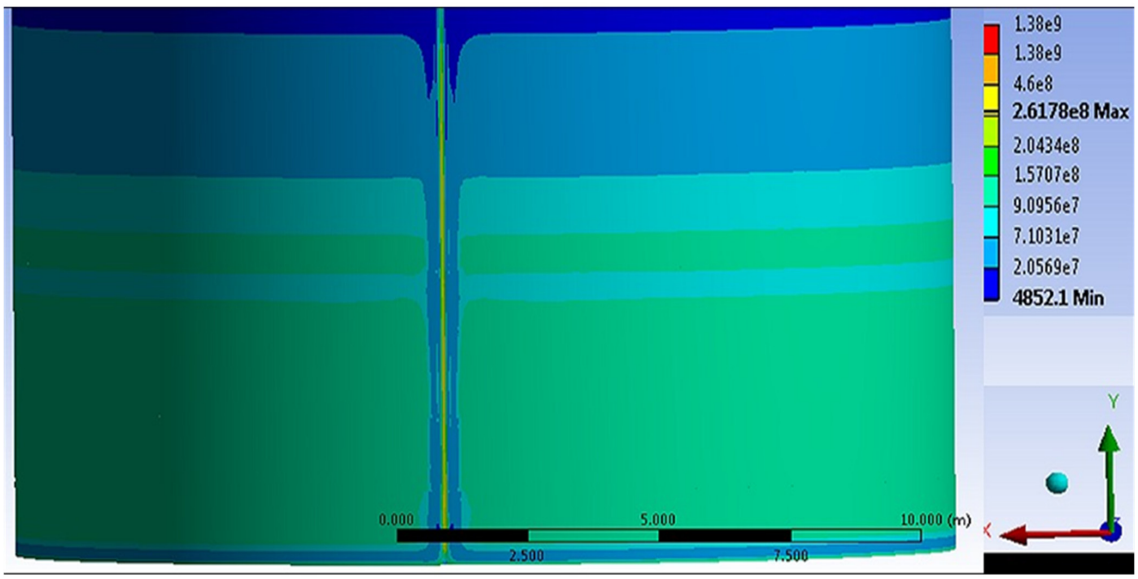

Figure 16. Distribution of equivalent stresses in the field joint zone with the joint imperfection at a = 50 cm; f = 15 cm.

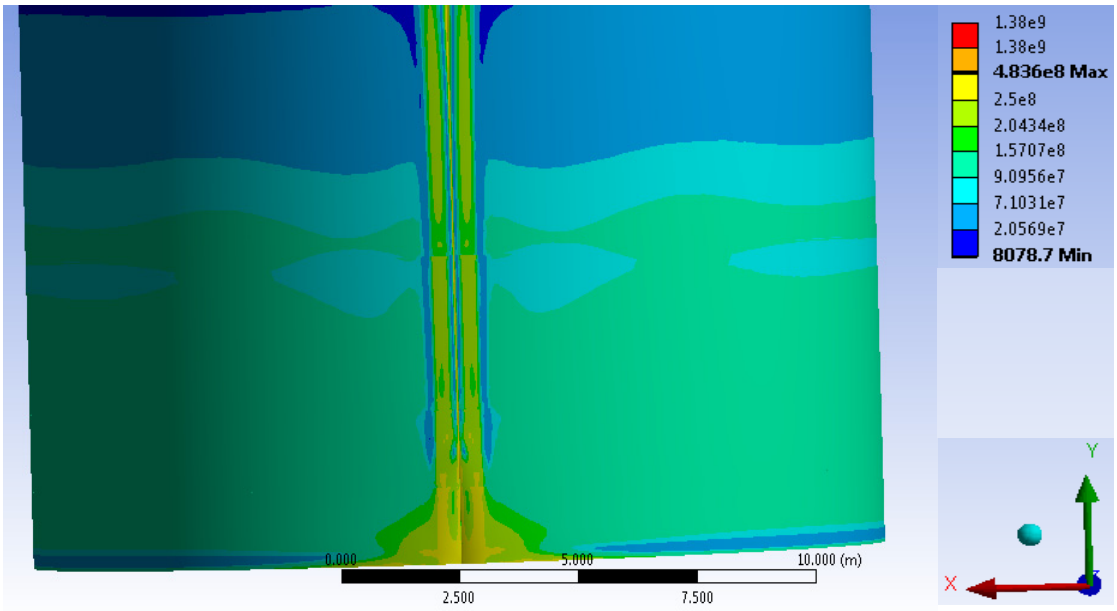

Figure 17. Distribution of equivalent stresses in the field joint zone with the joint imperfection at a = 50 cm; f = 10 cm.

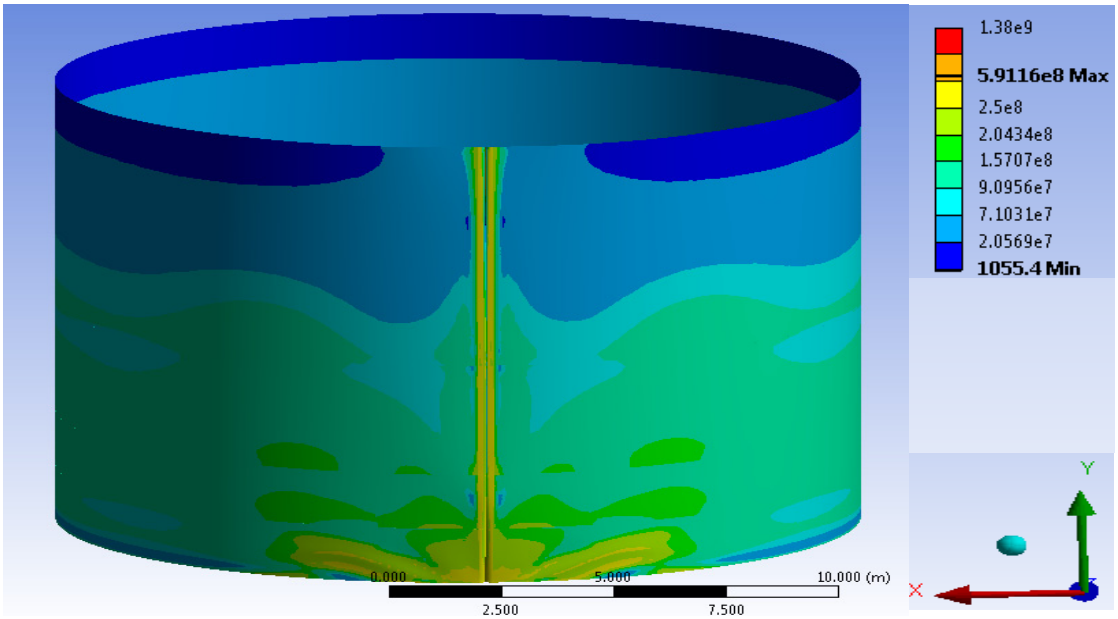

Figure 18. Distribution of equivalent stresses in the field joint zone with the joint imperfection at a = 15 cm; f = 10 cm.

Figures 15–18 show the equivalent stress calculation results for the following values of the field joint imperfection parameters:

$$(a,f) = (50;1);\ (a,f) = (50;15);$$

$$(a,f) = (50;10);\ (a,f) = (15;10). \quad (2)$$

The calculations showed that the highest stress concentration occurs at the tank base in the bottom junction with the tank wall near the field joint zone.

When calculating the stress concentration factor at the initial stage, the node with the highest equivalent stress value σ_{max} was found, as well as the nominal equivalent

stresses in the tank wall defect-free zone σ_θ. In this case, the stress concentration factor was determined from the following expression:

$$K = \frac{\sigma_{max}}{\sigma_\theta} \quad (3)$$

The stress concentration factor calculation results, using the ANSYS software package for various values of the dimensionless joint imperfection parameters, are presented in Table 2.

Table 2. The stress concentration factor K_σ calculation results in the cylindrical tank wall field joint imperfection zone [61].

Dimensionless Parameter $\xi=\frac{r_0}{\sqrt{R\cdot t}}$	**Dimensionless Values of the Joint Bend** $\varsigma=\frac{f}{t}$									
	1.25	**2.50**	**3.75**	**5.00**	**6.25**	**7.50**	**8.75**	**10.00**	**11.25**	**12.50**
1.87	1.487	1.761	1.775	1.818	1.859	1.889	1.917	1.946	1.977	2.009
1.68	1.495	1.763	1.783	1.836	1.873	1.905	1.937	1.971	2.002	2.037
1.49	1.502	1.765	1.796	1.851	1.885	1.920	1.956	1.994	2.030	2.066
1.31	1.550	1.769	1.815	1.865	1.903	1.945	1.987	2.030	2.071	2.108
1.12	1.661	1.775	1.836	1.883	1.928	1.973	2.016	2.059	2.116	2.172
0.93	1.753	1.784	1.855	1.904	1.954	2.014	2.066	2.128	2.201	2.273
0.75	1.761	1.800	1.872	1.933	1.995	2.061	2.146	2.234	2.311	2.384
0.56	1.762	1.820	1.899	1.974	2.062	2.176	2.284	2.380	2.468	2.546

From the results of calculating the stress concentration factor, according to Table 2, with an increase in the dimensionless parameters $\varsigma = \frac{f}{t}$ and $\xi = \frac{r_0}{\sqrt{R\cdot t}}$, the values K_σ increase.

Following relation (1), the interpolation polynomials for approximating the stress concentration factor are considered to depend on the following two independent variables: $K_\sigma = \alpha(\varsigma, \xi)$ The interpolation polynomials take the following form:

$$K_\sigma^T = \sum_{i=0}^{4} B_j(\varsigma)\xi^j\alpha; \quad (4)$$

where

$$\xi = \frac{r_0}{\sqrt{R\cdot t}};\ \varsigma = \frac{f}{t};\ B_j(\varsigma) = \sum_{j=0}^{B} b_j\varsigma^i$$

To construct this dependence, a two-stage application of the least square method was carried out. First, a polynomial approximation of the dependence K_σ (ξ) for each of the given values of the parameter ς was carried out and then, an approximate polynomial dependence of the obtained approximating polynomial factors on ξ was constructed. To construct the interpolation polynomial, the data of Table 2 were used [61].

$$\begin{aligned} K_\sigma = {} & (9 - 34.820\,\varsigma + 51.233\,\varsigma^2 + 4.828\,\varsigma^3 - 92.993\,\varsigma^4 + 110.249\,\varsigma^5 - 60.477\,\varsigma^6 + 16.520\,\varsigma^7 - 1.818\,\varsigma^8) + \\ & (9 - 68.83\,\varsigma + 224.56\,\varsigma^2 - 408.82\,\varsigma^3 + 454.87\,\varsigma^4 - 317.13\,\varsigma^5 + 135.45\,\varsigma^6 - 32.44\,\varsigma^7 + 3.339\,\varsigma^8)\xi + \\ & (9 - 73.80\,\varsigma + 257.28\,\varsigma^2 - 496.76\,\varsigma^3 + 581.33\,\varsigma^4 - 422.87\,\varsigma^5 + 187.123\,\varsigma^6 - 46.156\,\varsigma^7 + 4.86\,\varsigma^8)\xi^2 + \\ & (9 - 67.80\,\varsigma + 217.80\,\varsigma^2 - 390.58\,\varsigma^3 + 428.48\,\varsigma^4 - 294.90\,\varsigma^5 + 124.51\,\varsigma^6 - 29.514\,\varsigma^7 + 3.009\,\varsigma^8)\xi^3 + \\ & (9 - 68.87\,\varsigma + 224.86\,\varsigma^2 - 409.63\,\varsigma^3 + 456.04\,\varsigma^4 - 318.12\,\varsigma^5 + 135.94\,\varsigma^6 - 32.57\,\varsigma^7 + 3.353\,\varsigma^8)\xi^4 \end{aligned} \quad (5)$$

Thus, the interpolation polynomial was obtained that takes into account the cylindrical tank wall field joint imperfection + ns.

The stress concentration factor calculations, which depended on the geometric field joint imperfection dimensions, were performed using the ANSYS software package and using the polynomials (5). The comparison results are presented in Figures 19 and 20.

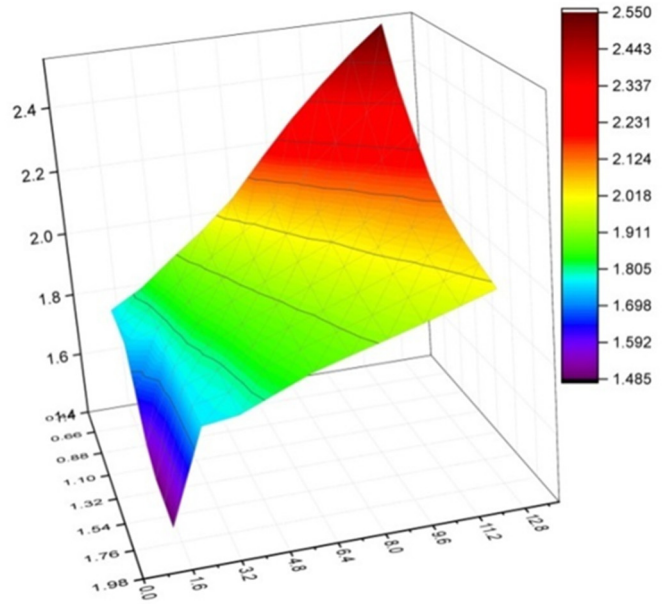

Figure 19. Dependence of the stress concentration factor on the geometric field joint imperfection dimensions ς, ξ.

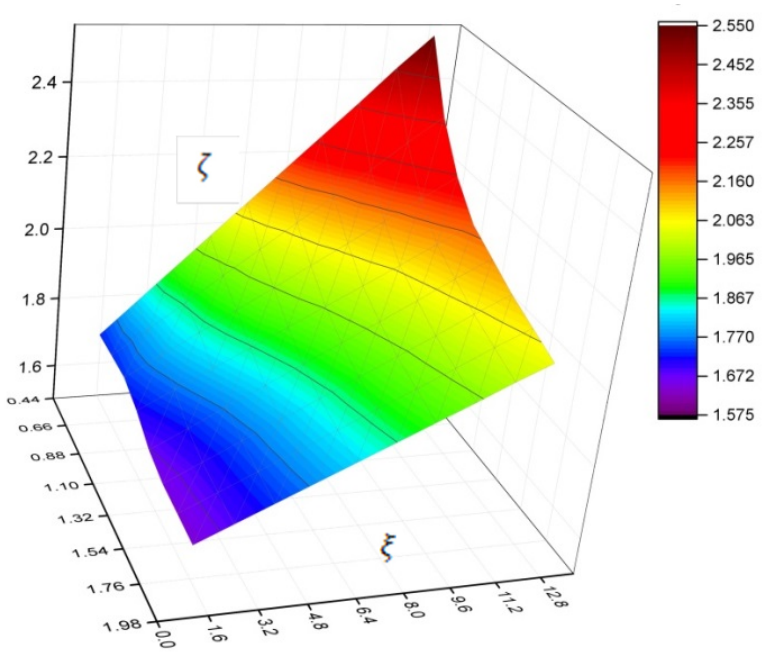

Figure 20. The interpolation polynomial surface from Equation (5) stress concentration factor.

As can be observed, the relative error of the results is no more than 1%, that is, it is within the acceptable limits [61].

The obtained dependences of the stress concentration factor K_σ on the dimensionless joint bend depth ς and the dimensionless joint imperfection width ξ, confirmed the determining influence on the stress concentration in the joint zone of its depth f. At the same time, the obtained dependences of the stress concentration factor on the joint imperfection parameters are important from the point of view of obtaining an engineering empirical calculation formula.

4. Discussion

Experimental tests of the tank wall fragment models with the field joint imperfections assessed the field joint zone's stress-strain state and established the stress concentration dependence in the joint zone on the bend, zone width and tank wall thickness.

The maximum hoop stresses in the joint zone in the model at the level of the main nominal stresses of 60.8 MPa with a 30 mm camber were 276 MPa and 358 MPa with a 50 mm camber. The maximum stress concentration in the joint zone was 4.54 for a 30 mm camber and 5.89 for a 50 mm camber. The maximum meridional stresses in the joint zone in the model with 30 mm and 50 mm cambers at the nominal stress level of 32 MPa amounted to 67 MPa and 78 MPa, respectively. At the same time, the results of the calculations of the equivalent stresses on the outer tank surface for various values of the tank wall field joint imperfection width and bend are shown in Figures 17–20. The above figures substantiate the initial assumption about the change in the stress field and significant stress concentrations in the field joint shape defect zone. From the results of the calculations of the stress concentration factor, according to Figures 17–20 and Table 2, it can be observed that when the dimensionless parameters ς and ξ, increase, the values of the stress concentration factor K_σ also increase.

The numerical analysis of tanks with joint imperfections estimated, in the ANSYS environment, the tank stress-strain state for various values of the joint bend parameters ς and ξ. The stress concentration factor dependence on the geometric dimensions of the tank wall imperfection, radius and thickness was also obtained. As a result of the calculations, the interpolation polynomial (5) was obtained, approximating the stress concentration factor K_σ, which can be used to assess the tank strength, durability and residual life. In addition, the obtained results can be used to normalize the limiting dimensions of the joint imperfections and establish the factor values, taking into account the features of the operation of structures at stress concentrations.

The resulting dependence of the stress concentration factor K_σ on the dimensionless joint bend depth ς and the dimensionless joint imperfection width ξ, confirmed the decisive influence on the stress concentration in the joint zone of the defect depth f. At the same time, the obtained stress concentration factor dependence on the joint imperfection parameters is important from the point of view of obtaining an engineering empirical calculation formula. Taking into account the limited application of the stress concentration dependence on the field joint imperfection size, subsequent studies should focus on obtaining a more advanced mathematical model for determining the stress concentration in the defect zone. In particular, such a model should take into account other operational factors and the joint imperfection shape.

It would be useful to note that this study is part of the research conducted as part of the study of the actual operation of vertical cylindrical tanks for oil and oil products. In the future, there is a need for full-scale studies of the stress-strain state of tank structures, with various geometric imperfections of field joints. At the same time, the obtained results can be used in the problems associated with assessing the strength, durability and residual life of tanks, taking into account the stress concentration in the field joint zone.

5. Conclusions

Experimental and theoretical studies were carried out to assess the influence of the vertical mounting joint zone of tanks on the stress-strain state of the defect zone. Thus, experimental tests of models of a tank wall fragment with an imperfection of the mounting joint evaluated the stress-strain state of the mounting joint zone and established the dependence of the stress concentration in the joint zone on the deflection.

Based on the major findings of this study, the following conclusions can be drawn:

- By testing the tank wall fragment models with field joint imperfections, the field joint zone's stress-strain state was assessed and the stress concentration dependence in the joint zone on the bend, zone width and tank wall thickness was established.

- The maximum hoop stresses in the joint zone in the model at the level of the main nominal stresses of 60.8 MPa with a 30 mm camber were 276 MPa and 358 MPa with a 50 mm camber. The maximum stress concentration in the joint zone was 4.54 for a 30 mm camber and 5.89 for a 50 mm camber.
- The maximum meridional stresses in the joint zone in the model with 30 mm and 50 mm cambers at the nominal stress level of 32 MPa amounted to 67 MPa and 78 MPa, respectively.
- Numerical analysis of tanks with joint imperfections estimated, in the ANSYS environment, the tank stress-strain state for various values of the joint bend parameters f/t and $a/\sqrt{Rt}$ and obtained the stress concentration factor dependence on the geometric dimensions of the tank wall imperfections, radius and thickness.
- As a result of the calculations, the interpolation polynomial (5) was obtained, approximating the stress concentration factor K_σ, which can be used to assess the tank's strength, durability and residual life, to normalize the limiting dimensions of the joint imperfection and establish the factor values, taking into account the features of the operation of structures at stress concentrations.

Author Contributions: Conceptualization, N.Z., U.S., R.F. and M.A.; methodology, U.S.; investigation, A.U. and B.D.; data curation, A.U. and N.Z.; writing—original draft preparation, K.I., A.K., A.M. and R.F.; writing—review and editing, K.I., A.K., A.M., K.B. and M.A.; supervision, K.B., G.K. and B.D.; project administration, N.Z.; funding acquisition, N.Z. All authors have read and agreed to the published version of the manuscript.

Funding: The study is funded by the authors of M. Auezov South Kazakhstan University.

Informed Consent Statement: Not applicable.

Data Availability Statement: Data sharing is not applicable to this article.

Conflicts of Interest: The authors declare no conflict of interest.

References

1. Kudabayev, R.; Suleimenov, U.; Ristavletov, R.; Kasimov, I.; Kambarov, M.; Zhangabay, N.; Abshenov, K. Modeling the Thermal Regime of a Room in a Building with a Thermal Energy Storage Envelope. *Math. Mod. Eng. Probl.* **2022**, *9*, 351–358. [CrossRef]
2. Zhangabay, N.; Abshenov, K.; Bakhbergen, S.; Zhakash, A.; Moldagaliyev, A. Evaluating the Effectiveness of Energy-Saving Retrofit Strategies for Residential Buildings. *Inter. Rev. Civ. Eng.* **2022**, *13*, 118–126. [CrossRef]
3. Suleimenov, U.; Zhangabay, N.; Utelbayeva, A.; Mohamad, N.; Moldagaliyev, A.; Abshenov, K.; Buganova, S.; Daurbekova, S.; Ibragimova, Z.; Dosmakanbetova, A. Determining the features of oscillations in prestressed pipelines. *East.-Eur. J. Enterp. Technol.* **2021**, *6*, 85–92. [CrossRef]
4. Tursunkululy, T.; Zhangabay, N.; Avramov, K.; Chernobryvko, M.; Suleimenov, U.; Utelbayeva, A.; Duissenbekov, B.; Aikozov, Y.; Dauitbek, B.; Abdimanat, Z. Strength analysis of prestressed vertical cylindrical steel oil tanks under operational and dynamic loads. *East.-Eur. J. Enterp. Technol.* **2022**, *2*, 14–21. [CrossRef]
5. Available online: https://tebiz.ru/mi/analiz-rynka-nefteproduktov-v-kazakhstane (accessed on 25 May 2022).
6. Mykhailo, H. Simulation of the stress-strain state of a cylindrical tank under the action of forced oscillations. *Procedia Struct. Integr.* **2022**, *36*, 79–86. [CrossRef]
7. Marwan, M.; Muthana, M.; Al-Jumialya, A.; Al-Muhammadia, A.; Ismaila, S. Development of a New Method for Reducing the Loss of Light Hydrocarbons at Breather Valve of Oil Tanks. *Energy Procedia* **2017**, *141*, 471–478. [CrossRef]
8. Hong, F.; Jiang, L.; Zhuo, Q.; Zhang, F.; Lu, X.; Ma, X.; Hao, J. Types of abnormal high-pressure gas reservoir in foreland basins of China. *J. Nat. Gas Geosci.* **2018**, *3*, 191–201. [CrossRef]
9. Duissenbekov, B.; Tokmuratov, A.; Zhangabay, N.; Yerimbetov, B.; Aldiyarov, Z. Finite-difference equations of quasistatic motion of the shallow concrete shells in nonlinear setting. *Curved Layer. Struct.* **2020**, *7*, 48–55. [CrossRef]
10. Borodin, K.; Zhangabay, N. Mechanical characteristics, as well as physical-and-chemical properties of the slag-filled concretes, and investigation of the predictive power of the metaheuristic approach. *Curved Layer. Struct.* **2019**, *6*, 236–244. [CrossRef]
11. Utelbaeva, A.B.; Ermakhanov, M.N.; Zhanabai, N.; Utelbaev, B.; Mel'deshov, A. Hydrogenation of benzene in the presence of ruthenium on a modified montmorillonite support. *Russ. J. Phys. Chem.* **2013**, *87*, 1478–1481. [CrossRef]
12. Filipov, V.; Prokhorov, V.; Argunov, S.; Buslaeva, I. The technical condition of the tanks for the storage of oil products of Yakutsknefteprodukt association. *News Univ. Constr.* **1993**, *7*, 13–16. Available online: https://cyberleninka.ru/article/n/tehnicheskaya-diagnostika-i-otsenka-ekspluatatsionnoy-nadezhnosti-rezervuarov-bolshogo-obema (accessed on 27 May 2022).

13. Biletsky, S.; Golinko, V. Industrial production of oversized welded sheet structures. *Nauk. Dumka.* **1983**, *272*. Available online: https://search.rsl.ru/ru/record/01001165555 (accessed on 25 May 2022).
14. Ivantsova, S.; Rakhmanin, A.; Tarasenko, M.; Silnitsky, P. The concept of risk analysis of tank structures. *Qual. Manag. Oil Gas Complex* **2011**, *3*, 31–35.
15. Mansurova, S.M.; Tlyasheva, R.R. Evaluation of the stress-strain state of a steel cylindrical tank, taking into account operational loads. *Oil Gas Bus. Electron. Sci. J.* **2014**, *1*, 2328–2334.
16. Suleimenov, U.; Zhangabay, N.; Utelbayeva, A.; Masrah, A.; Dosmakanbetova, A.; Abshenov, K.; Buganova, S.; Moldagaliyev, A.; Imanaliyev, K.; Duissenbekov, B. Estimation of the strength of vertical cylindrical liquid storage tanks with dents in the wall. *East.-Eur. J. Enterp. Technol.* **2022**, *7*, 6–20. [CrossRef]
17. Zhangabay, N.; Sapargaliyeva, B.; Utelbayeva, A.; Kolesnikov, A.; Aldiyarov, Z.; Dossybekov, S.; Esimov, E.; Duissenbekov, B.; Fediuk, R.; Vatin, N.I.; et al. Experimental Analysis of the Stress State of a Prestressed Cylindrical Shell with Various Structural Parameters. *Materials* **2022**, *15*, 4996. [CrossRef]
18. Li, Z.; Song, B.; Li, D. Safety Risk Recognition Method Based on Abnormal Scenarios. *Buildings* **2022**, *12*, 562. [CrossRef]
19. Thongchom, C.; Jearsiripongkul, T.; Refahati, N.; Roudgar Saffari, P.; Roodgar Saffari, P.; Sirimontree, S.; Keawsawasvong, S. Sound Transmission Loss of a Honeycomb Sandwich Cylindrical Shell with Functionally Graded Porous Layers. *Buildings* **2022**, *12*, 151. [CrossRef]
20. Kou, S.; Zhang, X.; Li, W.; Song, C. Dynamic Response Parameter Analysis of Steel Frame Joints under Blast Loading. *Buildings* **2022**, *12*, 433. [CrossRef]
21. Wang, J.; Kusunoki, K. Study on the Flexural Strength of Interior Thick Wall-Thick Slab Joints Subjected to Lateral Force Using Finite-Element Analysis. *Buildings* **2022**, *12*, 535. [CrossRef]
22. Fan, Y.; Hunt, J.; Wang, Q.; Yin, S.; Li, Y. Water tank modelling of variations in inversion breakup over a circular city. *Build. Environ.* **2019**, *164*, 106342. [CrossRef]
23. Martynenko, G.; Avramov, K.; Martynenko, V.; Chernobryvko, M.; Tonkonozhenko, A.; Kozharin, V. Numerical simulation of warhead transportation. *Def. Technol.* **2021**, *17*, 478–494. [CrossRef]
24. Wang, Z.; Hu, K.; Zhao, Y. Doom-roof steel tanks under external explosion: Dynamic responses and anti-explosion measures. *J. Constr. Steel Res.* **2022**, *190*, 107118. [CrossRef]
25. Rastgar, M.; Showkati, H. Buckling behavior of cylindrical steel tanks with concavity of vertical weld line imperfection. *J. Constr. Steel Res.* **2018**, *145*, 289–299. [CrossRef]
26. Fatma, M.; Aydın, K.; Mahyar, M.; Mahmut, K.; Cüneyt, A. Experimental analysis of the effect of dent variation on the buckling capacity of thin-walled cylindrical shells. *Thin-Walled Struct.* **2019**, *143*, 106259. [CrossRef]
27. Coramik, M.; Ege, Y. Discontinuity inspection in pipelines: A comparison review. *Measurement* **2017**, *111*, 359–373. [CrossRef]
28. Bannikov, R.; Smetannikov, O.; Trufanov, N.A. Method for calculating the amplitude of local conditional elastic stresses on the section of the tank wall with a shape defect in the form of dents. *Bull. Samara State Tech. Univ.* **2014**, *2*, 79–86. Available online: http://vestnik-teh.samgtu.ru/sites/vestnik-teh.samgtu.ru/files/auto/42_4_mashinostroenie_2014.pdf (accessed on 20 May 2022).
29. Dmitrieva, A.S.; Lyagova, A.A. Problems of assessing the technical condition of steel tanks with the "Dent" defect. In *Science and Youth in the XXI Century, Proceedings of 2nd All-Russian Scientific and Practical Conference*; Omsk State Technical University: Omsk, Russia, 2016; pp. 138–142. Available online: https://www.elibrary.ru/item.asp?id=28085497 (accessed on 25 May 2022).
30. Mariusz, M.; Michal, P.; Janusz, S.; Krzyszt, T. Corrosion Durability Estimation for Steel Shell of a Tank Used to Store Liquid Fuels. *Procedia Eng.* **2017**, *172*, 723–730. [CrossRef]
31. Song, Z.; Komvopoulos, K. Contact mechanics analysis of oscillatory sliding of a rigid fractal surface against an elastic-plastic half-space. *Philos. Mag.* **2014**, *94*, 3215–3233. [CrossRef]
32. Hagihara, S.; Tsunori, M.; Ikeda, T.; Miyazaki, N. Application of meshfree method to elastic-plastic fracture mechanics parameter analysis. *Comput. Model. Eng. Sci.* **2007**, *17*, 63–72. [CrossRef]
33. Sun, J. Hard particle force in a soft fracture. *Sci. Rep.* **2019**, *9*, 3065. [CrossRef] [PubMed]
34. Zhang, Y.M.; Tan, T.K.; Xiao, Z.; Zhang, W.G.; Ariffin, M.Z. Failure Assessment on Offshore Girth Welded Pipelines due to Corrosion Defects. *Fatigue Fract. Eng. Mater. Struct.* **2016**, *39*, 453–466. [CrossRef]
35. Yi, D.; Sridhar, I.; Xiao, Z.; Kumar, S. Fracture capacity of girth welded pipelines with 3D surface cracks subjected to biaxial loading conditions. *Int. J. Press. Vessel. Pip.* **2012**, *92*, 115–126. [CrossRef]
36. Kolesov, A.I.; Ageeva, M.A. Residual resource of steel tanks for chemistry and petrochemistry that have worked out their standard operating life. *Bull. MSCU* **2011**, *1*, 388–391.
37. TP-704-1-167-84. Steel Vertical Cylindrical Tank for Oil and Oil Products with a Volume of 3000 m^3. Album I. Metal Tank Structures. Available online: https://meganorm.ru/Data2/1/4293833/4293833208.pdf (accessed on 28 May 2022).
38. GOST 27069-86. Metallic Ferroalloys, Chromium and Manganese. Methods for Determining Carbon. Available online: https://docs.cntd.ru/document/1200008986 (accessed on 25 May 2022).
39. GOST 1497-84. Metals. Tensile Test Methods. Available online: https://docs.cntd.ru/document/1200004888 (accessed on 25 May 2022).
40. Volokitina, I.; Siziakova, E.; Fediuk, R.; Kolesnikov, A. Development of a Thermomechanical Treatment Mode for Stainless-Steel Rings. *Materials* **2022**, *15*, 4930. [CrossRef] [PubMed]

41. Kolesnikov, A.S. Kinetic Investigations into the Distillation of Nonferrous Metals during Complex Processing of Waste of Metallurgical Industry. *Rus. J. Non-Ferr. Met.* **2015**, *56*, 1–5. [CrossRef]
42. Volokitin, A.; Naizabekov, A.; Volokitina, I.; Kolesnikov, A. Changes in microstructure and properties of austenitic steel aisi 316 during high-pressure torsion. *J. Chem. Technol. Metall.* **2022**, *57*, 809–815.
43. Kuatbay, Y.; Nurumgaliyev, A.; Shabanov, Y.; Zayakin, O.; Gabdullin, S.; Zhuniskaliyev, T. Melting of high-carbon ferrochrome using coal of the saryadyr deposit. *Metalurgija* **2022**, *61*, 367–370.
44. Kolesnikov, A.S. Thermodynamic simulation of silicon and iron reduction and zinc and lead distillation in zincoligonite ore-carbon systems. *Russ. J. Non-Ferr. Met.* **2014**, *55*, 513–518. [CrossRef]
45. Boikov, A.; Payor, V.; Savelev, R.; Kolesnikov, A. Synthetic data generation for steel defect detection and classification using deep learning. *Symmetry* **2021**, *13*, 1176. [CrossRef]
46. Kolesnikov, A.S.; Sergeeva, I.V.; Botabaev, N.E.; Al'Zhanova, A.Z.; Ashirbaev, K.A. Thermodynamic simulation of chemical and phase transformations in the system of oxidized manganese ore—Carbon. *Izv. Ferr. Metall.* **2017**, *60*, 759–765. [CrossRef]
47. Volokitina, I.; Kolesnikov, A.; Fediuk, R.; Klyuev, S.; Sabitov, L.; Volokitin, A.; Zhuniskaliyev, T.; Kelamanov, B.; Yessengalie, V.D.; Yerzhanov, A.; et al. Study of the Properties of Antifriction Rings under Severe Plastic Deformation. *Materials* **2022**, *15*, 2584. [CrossRef] [PubMed]
48. Kolesnikov, A.; Fediuk, R.; Amran, M.; Klyuev, S.; Klyuev, A.; Volokitina, I.; Naukenova, A.; Shapalov, S.; Utelbayeva, A.; Kolesnikova, O.; et al. Modeling of Non-Ferrous Metallurgy Waste Disposal with the Production of Iron Silicides and Zinc Distillation. *Materials* **2022**, *15*, 2542. [CrossRef] [PubMed]
49. Vasilyeva, N.; Fedorova, E.; Kolesnikov, A. Big Data as a Tool for Building a Predictive Model of Mill Roll Wear. *Symmetry* **2021**, *13*, 859. [CrossRef]
50. Rensky, A.B.; Baranov, D.S. *Strain Measurement of Building Structures and Materials*; Stroyizdat: Moscow, Russia, 1977; 239p, Available online: https://e-catalog.nlb.by/Record/BY-NLB-rr29377930000 (accessed on 25 May 2022).
51. Kolesnikov, A.; Fediuk, R.; Kolesnikova, O.; Zhanikulov, N.; Zhakipbayev, B.; Kuraev, R.; Akhmetova, E.; Shal, A. Processing of Waste from Enrichment with the Production of Cement Clinker and the Extraction of Zinc. *Materials* **2022**, *15*, 324. [CrossRef]
52. Zhakipbaev, B.Y.; Zhanikulov, N.N.; Kuraev, R.M.; Shal, A.L. Review of technogenic waste and methods of its processing for the purpose of complex utilization of tailings from the enrichment of non-ferrous metal ores as a component of the raw material mixture in the production of cement clinker. *Rasayan J. Chem.* **2021**, *14*, 997–1005. [CrossRef]
53. Serikbaev, B.E.; Zolkin, A.L.; Kenzhibaeva, G.S. Processing of Non-Ferrous Metallurgy Waste Slag for its Complex Recovery as a Secondary Mineral Raw Material. *Refract. Ind. Ceram.* **2021**, *62*, 375–380. [CrossRef]
54. Kolesnikov, A.S.; Zhanikulov, N.N.; Zhakipbayev, B.Y.; Kolesnikova, O.G.; Kuraev, R.M. Thermodynamic modeling of the synthesis of the main minerals of cement clinker from technogenic raw materials. *Kompleksnoe Ispol'zovanie Mineral'nogo Syr'a. (Complex Use Miner. Resour.)* **2021**, *318*, 24–34. [CrossRef]
55. Zhanikulov, N.N.; Khudyakova, T.M.; Taimasov, B.T. Receiving portland cement from technogenic raw materials of South Kazakhstan portlandcement. *Eurasian Chem. Technol. J.* **2019**, *21*, 334–340. [CrossRef]
56. GOST 50779.21-2004. Statistical Methods. Rules for Determining and Methods for Calculating Statistical Characteristics from Sample Data. Part 1. Normal Distribution. Available online: https://docs.cntd.ru/document/1200035333 (accessed on 25 May 2022).
57. Makul, N.; Fediuk, R.; Amran, M.; Zeyad, A.M.; Murali, G.; Vatin, N.; Klyuev, S.; Ozbakkaloglu, T.; Vasilev, Y. Use of Recycled Concrete Aggregates in Production of Green Cement-Based Concrete Composites: A Review. *Crystals* **2021**, *11*, 232. [CrossRef]
58. Fediuk, R.S.; Yushin, A.M. The use of fly ash the thermal power plants in the construction. *IOP Conf. Ser. Mater. Sci. Eng.* **2015**, *93*, 012070. [CrossRef]
59. Abid, S.R.; Murali, G.; Amran, M.; Vatin, N.; Fediuk, R.; Karelina, M. Evaluation of Mode II Fracture Toughness of Hybrid Fibrous Geopolymer Composites. *Materials* **2021**, *14*, 349. [CrossRef] [PubMed]
60. Zhangabay, N.; Sapargaliyeva, B.; Suleimenov, U.; Abshenov, K.; Utelbayeva, A.; Kolesnikov, A.; Baibolov, K.; Fediuk, R.; Arinova, D.; Duissenbekov, B.; et al. Analysis of Stress-Strain State for a Cylindrical Tank Wall Defected Zone. *Materials* **2022**, *15*, 5732. [CrossRef] [PubMed]
61. Suleimenov, U.; Zhangabay, N.; Abshenov, K.; Utelbayeva, A.; Imanaliyev, K.; Mussayeva, S.; Moldagaliyev, A.; Yermakhanov, M.; Raikhanova, G. Estimating the stressed-strained state of the vertical mounting joint of the cylindrical tank wall taking into consideration imperfections. *East.-Eur. J. Enterp. Technol.* **2022**, *3*, 14–21. [CrossRef]